applied sciences

MDPI

Article

Parameters Calibration of Discrete Element Model for Corn Straw Cutting Based on Hertz-Mindlin with Bonding

Wenhang Liu †, Qiang Su †, Mei Fang, Jianchao Zhang, Wenjie Zhang * and Zhihong Yu

College of Mechanical and Electrical Engineering, Inner Mongolia Agricultural University, Hohhot 010018, China
* Correspondence: imauzwj@imau.edu.cn
† These authors contributed equally to this work.

Abstract: Aiming at the lack of a precise discrete element model in the simulation analysis of corn straw crushing, this paper established bond models with different structure and particle models with different properties of corn straw based on Hertz-Mindlin with bonding, and verified the discrete element model by combining physical test and simulation optimization design methods. Firstly, this study generates the bonded particle models based on Hertz-Mindlin with bonding for epidermis-epidermis, inner flesh-internal flesh, and epidermis-internal flesh, respectively. The bonding parameters of the model are calibrated with the help of a bending damage test, bending damage simulation test, and actual test with 2 mm/min speed. It shows that the maximum destructive force errors of the epidermis and inner flesh are 2.4% and 1.6%, respectively. On this basis, a discrete element model of corn straw is established by combining the calibrated parameters of the bonding parameters of epidermis—epidermis, inner flesh—inner flesh, and epidermis—inner flesh bond. The bending failure test shows that the mechanical properties of corn straw are similar between the simulated test and the actual test, and the maximum destructive power is 288 N and 292 N, respectively. The relative error is 1.36%. The feasibility of the discrete element model for simulation analysis is verified, which shows that the established discrete element model can be applied to the simulation analysis of corn straw cutting and crushing process.

Keywords: corn straw; discrete element method; maximum breaking force; bonding model

check for updates

Citation: Liu, W.; Su, Q.; Fang, M.; Zhang, J.; Zhang, W.; Yu, Z. Parameters Calibration of Discrete Element Model for Corn Straw Cutting Based on Hertz-Mindlin with Bonding. *Appl. Sci.* **2023**, *13*, 1156. https://doi.org/10.3390/app13021156

Academic Editor: Rafael López Núñez

Received: 2 December 2022
Revised: 11 January 2023
Accepted: 11 January 2023
Published: 15 January 2023

Copyright: © 2023 by the authors. Licensee MDPI, Basel, Switzerland. This article is an open access article distributed under the terms and conditions of the Creative Commons Attribution (CC BY) license (https://creativecommons.org/licenses/by/4.0/).

1. Introduction

Corn is one of the major food crops in China, and with the increase in planting area, the amount of corn straw resources as a by−product of agricultural production is also increasing, accounting for 42.87% of the total straw of the three major food crops [1]. In the process of achieving "carbon peaking" and "carbon neutrality", the potential use of maize straw is increasingly valued, playing a huge role in the manufacture of biofuels [2], livestock feed [3–5], soil nutrients [6–8], and composite materials [9–11], and straw cutting and shredding are prerequisites for the effective use of crop straws, from silking to shredding for field return [12–14]. The coarse fiber of corn straws at maturity formed, and the cutting process, requires a large cutting force to ensure that the shredded segments of corn straws meet the requirements [15], so the development of cutting and shredding equipment dedicated to corn straws to improve the shredding quality of corn straws is essential to promote the comprehensive utilization of corn straws. The discrete element method can reveal the interaction mechanism between cutting components and corn straw, which shows great advantages in designing and optimizing key components of the corn straw shredder [16].

The discrete element method is applied to the study of straw cutting and crushing, the difficulty is how to accurately establish the straw model and calibrate the parameter values. Zhao Shuhong et al. [17] established multiple spherical particles with the same diameter and generated a discrete element model of straw by means of spherical particle

stacking, and the resulting model was a rigid body; Wang Ruili et al. [18] used the same spherical particles to build a discrete element model of round bale corn straw breaking and calibrated the contact parameters between materials using the stacking angle method; Fang Mei et al. [19] conducted a study on corn straw, straw node and inner flesh mixtures to the contact parameters were calibrated, and the discrete element models of straws, straw nodes, and inner flesh were developed separately by using the spherical particle stacking method. These studies considered corn straw as homogeneous material and used the same kind of particle spheres to build the discrete element model, which ignored the mechanical properties of the different structures of corn straw skin and inner flesh and the discrete element model could not be simulated for fragmentation. In order to ensure the accuracy of the discrete element model, some scholars selected different contact models to establish the discrete element model of crop straws: For example, Li Xian Zhang et al. [20] used the Hertz-Mindlin with JKR model to establish the discrete element model for the epidermis and inner flesh of corn straws by combining mechanical tests and numerical models, and conducted straw baling tests; Wang Weiwei et al. [21] used the Hertz-Mindlin with JKR model to calibrate the parameters of the discrete element simulation model for dense forming of corn straw meal, and verified the availability of the relevant parameters through the corn straw meal mold hole compression test. The accuracy of the discrete element model was further improved by building separate discrete element models for different structures of corn straw (epidermis and inner flesh), but the method was mostly used for compression molding simulations. In order to explore more deeply the accuracy of the discrete element method to simulate corn straw crushing, Hou Jie [22], Shi Ruijie [23], Zhang Fengwei [24], and Geng Duanyang [25] used the discrete element method Hertz-Mindlin with bonding to construct the corresponding straw models, respectively, which can reflect its relevant mechanical properties through bond rupture when subjected to external forces. Therefore, this model can be considered for discrete element modeling of corn straw fragmentation.

The differentiation of relevant parameters of different structures in the process of building discrete element models can further improve the accuracy and reliability of simulation tests. In this paper, the discrete element Hertz-Mindlin, with bonding and different kinds of particle spheres, are used to build the discrete element model of corn straw skin and inner flesh, and the bonding parameters of the discrete element model are calibrated by comparing the bending damage test with the simulation test. Then the cutting and throwing test of corn straw is carried out, and the throwing distance of the broken segments of corn straw is measured to further verify the accuracy of the simulation in order to provide a parameter basis for studying the cutting and throwing mechanism of corn straw and the optimization design of the shredder.

2. Materials and Methods

2.1. Test Materials

The corn straw of Zhongbang 1088 maize, which is commonly grown in the northern region (China), is selected for the test, and its cross and longitudinal sections are shown in Figure 1. The corn straw with more uniform diameter, that is thicker and straighter, and has no obvious damage are selected from the root upwards, and the diameter, inner flesh diameter, and skin thickness of the corn straw are measured by using vernier calipers, which have a moisture content of 53% to 65%, the density of 613 kg/m^3, the skin thickness of about 2.5 mm, the density of about 698 kg/m^3, and the inner flesh thickness of about 23.5 mm and the density of about 70 kg/m^3.



Figure 1. Shape of corn straws.

2.2. Hertz-Mindlin and Bonding Parameter Model

Using Hertz-Mindlin with bonding as a contact model between particles, bonding bonds are generated between disconnected neighboring particles to limit the relative motion between particles. Under the action of external forces, the particle spheres produce normal and shear displacements, and the bonding bond is analyzed from the force point of view by the changes in bending moment, torque, tension, pressure, and shear causing the bond breakage, and the bonding bond is established in the discrete element by the parameters of normal stiffness, shear stiffness, normal critical stress, and shear critical stress, so the force required for bond breakage is adjusted by the changes in the values of the bonding parameters, as shown in Figure 2. The bond will be broken when the stress between adjacent particles reaches its maximum value. Therefore, this contact model is suitable for simulating problems such as the breaking and fracture of corn straw under external forces [26].

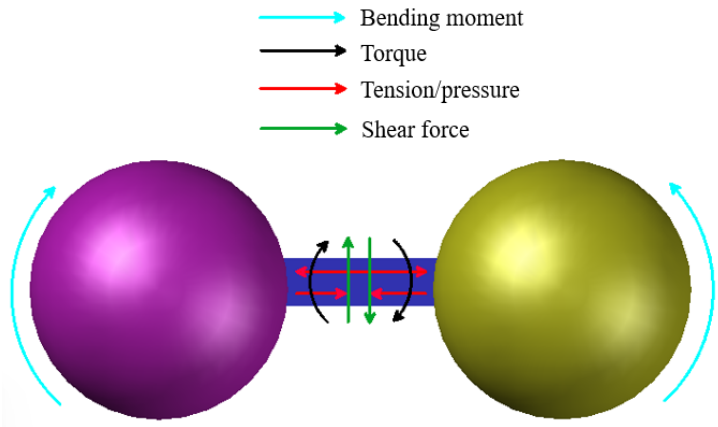


Figure 2. Interaction forces between Hertz-Mindlin particles.

The bond parameters of the epidermis, inner flesh, and epidermis-internal flesh of corn straw are critical to the formation of the bond bonds between the particles in the corn straw model and determine the accuracy of the discrete element model of corn straw. If the stiffness value of the bonding parameter is less than the sum of external forces on the particles, it will cause the straw model to collapse. On the contrary, if the stiffness value of the bonding parameter is too large, the elastic deformation of the contact part between the particles exceeds the critical value of the bonding bond, causing the particle model to blow up. The main parameters of the inter−particle bonding bond when the Hertz-Mindlin with Bonding model is used in the study are normal stiffness Kn, shear stiffness Ks, normal critical stress σ, and shear critical stress γ. The above parameters cannot be obtained directly by experiment, according to the Hertz-Mindlin with Bonding model theory [27] and Moore's shear theory [28], as Equation (1) is shown. Combined with the mechanical compression and shear tests of different structures of corn straw in the

previous phase of this project group and the related analysis [29,30], the range of values of different bonding parameters is calculated and shown in Table 1.

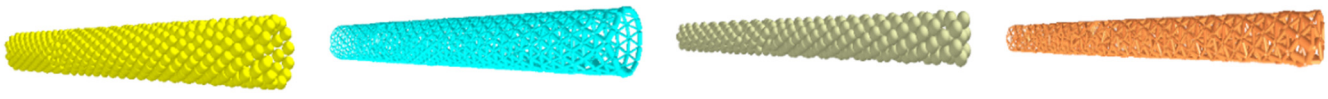
$$\begin{cases} K_{\mathrm{n}} = \frac{4}{3}\left(\frac{1-\varepsilon_a^2}{E_a} + \frac{1-\varepsilon_b^2}{E_b}\right)^{-1}\left(\frac{r_a+r_b}{r_a r_b}\right)^{-\frac{1}{2}} \\ K_{\mathrm{s}} = \left(\frac{1}{2} \sim \frac{2}{3}\right)K_{\mathrm{n}} \\ \sigma = \frac{F}{\pi R^2} \\ \gamma = c + \sigma \tan\varphi \end{cases} \quad (1)$$

where ε_a, ε_b is the particle Poisson's ratio; E_a, E_b is the modulus of elasticity of particles, MPa; r_{a}, r_{b} is the particle radius, mm; F is the critical pressure, N; R is the compressed cotton radius, mm; C is the stem cohesion, MPa; and φ is the angle of internal friction (°).

Table 1. Corn straw bonding parameters.

Bonding Parameters	Epidermal Granules−Epidermal Granules	Core Granules−Core Granules	Core Granules−Epidermal Granules
Normal stiffness/(N·m^{-1})	3.9×10^9 5.2×10^9 6.5×10^9 7.8×10^9 9.1×10^9	2×10^8 3.8×10^8 5.6×10^8 7.4×10^8 9.2×10^8	2×10^7 3.5×10^8 5×10^8 6.5×10^8 6.5×10^8
Shear stiffness/(N·m^{-1})	2.9×10^8 4.4×10^8 5.9×10^8 7.4×10^8 8.9×10^8	2.0×10^8 3.0×10^8 4.0×10^8 5.0×10^8 6.0×10^8	6×10^6 1.95×10^7 3.3×10^7 4.65×10^7 6×10^7
Normal critical stress/Pa	1.0×10^8 2.1×10^8 3.2×10^8 4.3×10^8 5.4×10^8	1.5×10^7 2.5×10^7 3.5×10^7 4.5×10^7 5.5×10^7	4.5×10^5 5.0×10^5 5.5×10^5 6.0×10^5 6.5×10^5
Shear critical stress/Pa	1.0×10^7 2.0×10^7 3.0×10^7 4.0×10^7 5.0×10^7	2.5×10^5 3.5×10^5 4.5×10^5 5.5×10^5 6.5×10^5	2.5×10^5 3.0×10^5 3.5×10^5 4.0×10^5 4.5×10^5

At the mature stage, corn straw show different degrees of lignification and fibrosis, and the mechanical properties of different structures are different. Discrete element models of epidermis and inner flesh are established by using the approximation method, as shown in Figure 3.



(**a**) (**b**) (**c**) (**d**)

Figure 3. Bonding bond model. (**a**) Surface skin discrete element model. (**b**) Surface skin particle bonding. (**c**) Inner flesh discrete element model. (**d**) Inner flesh particle bonding.

The discrete element model of the epidermis and inner flesh is established by the particle substitution method, and the modeling process is shown in Figure 4, based on Solidworks, to establish the geometric model of the epidermis and inner flesh of corn

straw, and the mesh division is carried out by a combination of tetrahedral and hexahedral methods; the divided model is imported into EDEM software, and the particle factory is established to achieve rapid particle filling, and the particle database program is compiled using Visio Studio to modify the particle volume fraction and particle diameter. The particle volume fraction and particle diameter are modified by compiling the particle database program with Visio Studio, setting the epidermal particle diameter to 1 mm and the inner flesh particle diameter to 2.5 mm, and exporting the position coordinates of the particles of different structures. The position coordinates of the different structural particles are imported into the Hertz-Mindlin with the bonding replacement particle file, and the bonding bonds are generated separately for the epidermal and inner flesh particles of corn straw in EDEM. Finally, the values of bonding parameters, such as normal stiffness, shear stiffness, normal critical stress, and shear critical stress are set in the EDEM.

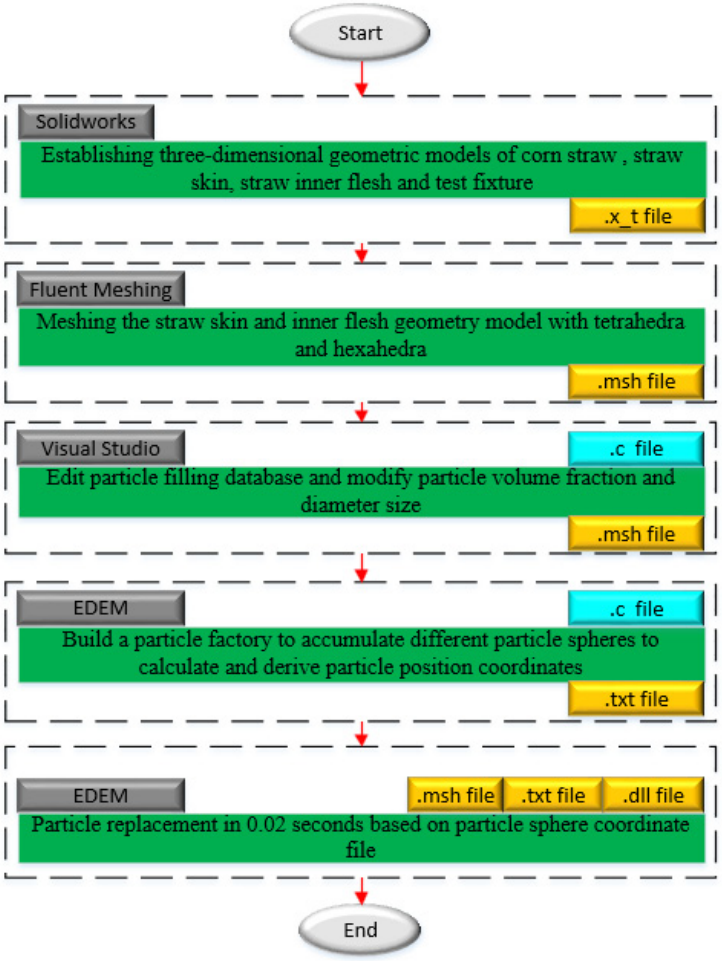


Figure 4. Method of building discrete element model of specimen.

2.3. Bending Damage Test

The bending damage test of corn straw is carried out using a mass spectrometer (TMS−Pro), with the length of the epidermis and inner flesh specimens being 100 mm and the distance between the two pivot points of the test stand support base being 80 mm, and the specimens are placed steadily on the support stand, as shown in Figure 5. First the pressure plate is made vertical down close to the specimen, but not in contact with it, and then the loading speed of 2 mm/min is adjusted, and the straw in the texture of the load force is applied by the instrument after extrusion deformation and bending deformation until fracture. The bending damage force at the time of straw fracture is the maximum load, and finally, the maximum load value of the epidermis and inner flesh is recorded.

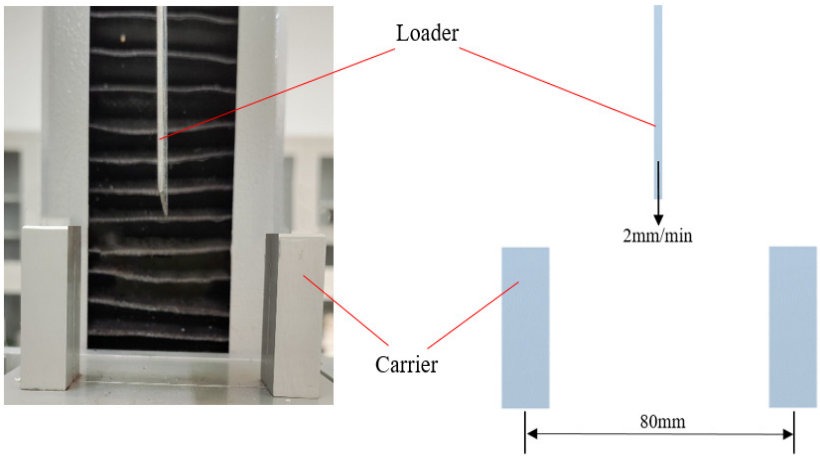


Figure 5. Bending test setup and geometric model.

2.4. Discrete Element Simulation of Bending Test

In the bending damage simulation, parameters such as the motion state, material properties, and position relations of the loaded structural components need to be set, and the geometric models of the support plate and pressure plate in the simulation are drawn by Solidworks software, and their relative positions are the same as those of the actual test, and the models of the pressure plate and support frame are imported into ANSYS ICEM for meshing, and the pressure plate in the simulation process moves at a 2 mm/min velocity vertical horizontal plane moving downward at a uniform speed, and the time step calculated for the simulation is 6.5×10^{-7} s. According to the literature [31,32], and combined with the stacking angle test of corn straw, the contact parameters between different materials are derived, as shown in Table 2.

Table 2. Contact parameters of different structures of corn straw.

Contact Parameters	Epidermis—Steel	Inner Flesh—Steel	Epidermis—Epidermis	Epidermis—Inner Flesh	Inner Flesh—Inner Flesh
Crash recovery factor	0.608	0.358	0.481	0.385	0.301
Static friction coefficient	0.328	0.378	0.211	0.432	0.487
Rolling friction coefficient	0.112	0.128	0.096	0.118	0.142

2.5. Verification Experimental

The corn straw chopping machine is shown in Figure 6. The working principle of the machine is as follows: corn straw is forced by the forward motion of the chain plate into the cutting device, the chopped straw broken section is forced by gravity and the dynamic knife into the throwing chamber, and the straw broken section in the role of the throwing mechanism is thrown out. At the beginning of the test, a quantity of corn straw is put on the conveyor chain plate to make the machine work at the speed set in the test. When the speed is stable, the gearbox is opened to control the forward gear lever of the conveyor chain plate, so that the straws are first cut into evenly broken segments and then enter the throwing room, and the throwing mechanism sends the broken segments outside the machine.



Figure 6. Corn straw shredder. Note: 1. walking device, 2. transmission device, 3. throwing chamber, 4. cutting device, 5. conveying device, and 6. conveying chain plate.

To demonstrate the feasibility of the discrete element simulation method to study the corn straw cutting and throwing process, a cutting and throwing test is designed, as shown in Figure 7. The coupled CFD−DEM simulation of the corn straw cutting and throwing test is carried out considering that the actual working process will generate high−speed flowing airflow inside the throwing chamber. A three−dimensional model of the cutting and throwing device is established using SolidWorks software, Fluent was used to mesh the simulation model of the test bench, and the number of mesh quality requirements should not be too much, and the cutting and throwing device was simplified for accurate calculation results and reduced calculation time, and the Eulerian-Eulerian model was used to realize the interaction between airflow and particles, and the flow of gas and particles conformed to the actual law of motion, and the 3D model was imported into EDEM. The boundary conditions are set in EDEM, and the parameters of the Hertz-Mindlin model and the Hertz-Mindlin with bonding model are set, and the Fluent flow field information is passed to EDEM for coupling through the API interface, and a discrete element model of corn straw is established and simulated according to the above bonding parameters, as shown in Figure 8. A single−factor control test is set up to compare the throwing distances of straw chopped segments at different speeds (600, 625, 650, 675, and 700 r/min) in the simulated and actual tests, and the relative errors of the throwing distances are calculated.

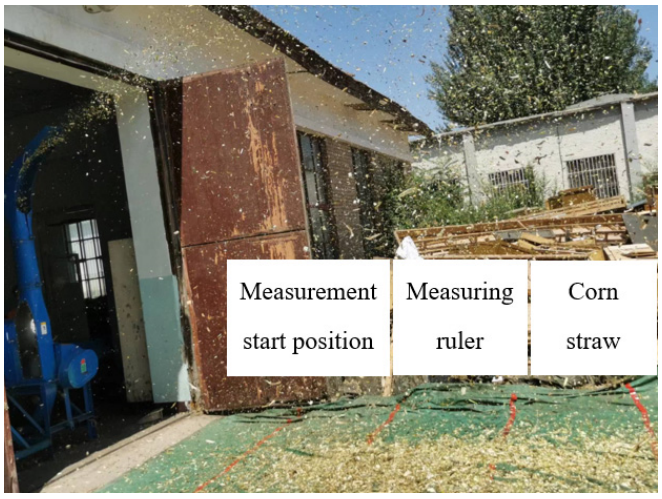


Figure 7. Test site.

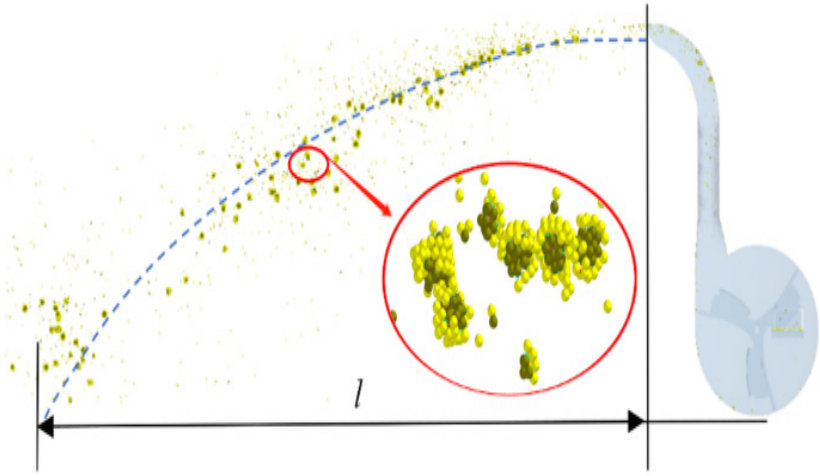


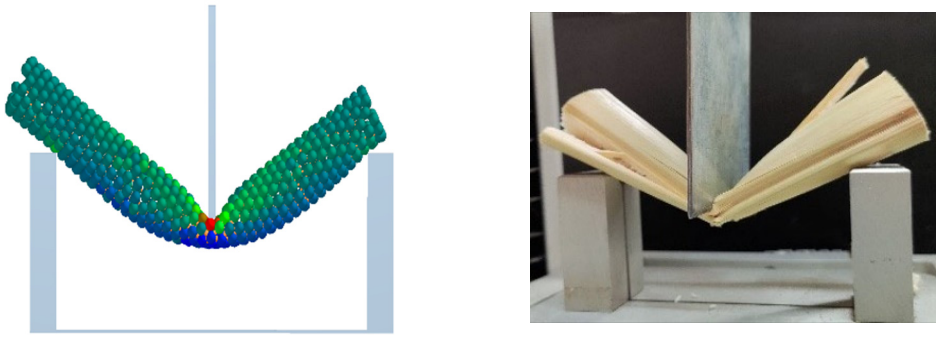
Figure 8. CFD−DEM coupled simulation cutting and throwing test.

3. Results and Discussion

To ensure that the strength and deformation of the discrete element model are consistent with the actual test results, the bonding parameters are calibrated according to the biological properties of corn straw itself divided into three different structures (epidermis, inner flesh, and epidermis-internal flesh) to further optimize the established discrete element model. Three sets of bonding parameters are coded before the simulation tests, with five sets of replicate tests at the central group level and thirty sets of simulation tests for different structures of straw, respectively.

3.1. Optimization of Corn Straw Epidermal Bonding Parameters

A straw with a diameter of about 28.5 mm in the middle section of corn straw is selected, and the inner flesh is removed to make a cylinder specimen with a length of 100 mm, and a model of the same size is built in the discrete element for the virtual bending damage test, as shown in Figure 9.



(**a**) (**b**)

Figure 9. Straw skin bending test. (**a**) Epidermal discrete element bending test; (**b**) epidermal physical bending test.

In order to ensure the reliability of the parameter range in the parameter calibration process and avoid the adverse effects caused by the parameter taking values beyond the range, the response surface test is designed according to the central combination design principle. With F_1 as the response value and X_1 (normal stiffness), X_2 (shear stiffness), X_3 (normal critical force), and X_4 (shear critical force) as independent variables, the bending damage simulation test and analysis of corn straw are carried out, and the test factors and levels are shown in Table 3, and the bending damage force test scheme and results are shown in Table 4.

Table 3. Factors and levels of epidermal bonding model simulation tests.

Code Value	Bonding Parameters			
	X_1/(N·m^{-1})	X_2/(N·m^{-1})	X_3/MPa	X_4/MPa
−2	3.9×10^9	2.9×10^8	100	10
−1	5.2×10^9	4.4×10^8	210	20
0	6.5×10^9	5.9×10^8	320	30
1	7.8×10^9	7.4×10^8	430	40
2	9.1×10^9	8.9×10^8	540	50

Table 4. Simulation test design and results of epidermal bonding model.

Serial Number	X_1/(N·m^{-1})	X_2/(N·m^{-1})	X_3/MPa	X_4/MPa	Destructive Power (F_1)/N
1	5.2×10^9	7.4×10^8	210	40	119.2
2	7.8×10^9	4.4×10^8	430	40	117.8
3	6.5×10^9	5.9×10^8	320	30	159.3
4	7.8×10^9	7.4×10^8	210	20	190.9
5	5.2×10^9	4.4×10^8	430	40	98.3
6	5.2×10^9	7.4×10^8	430	20	112.4
7	6.5×10^9	5.9×10^8	320	30	139.5
8	9.1×10^9	5.9×10^8	320	30	136.9
9	6.5×10^9	5.9×10^8	100	30	97.4
10	6.5×10^9	5.9×10^8	320	30	138.4
11	6.5×10^9	5.9×10^8	540	30	92.9
12	6.5×10^9	2.9×10^8	320	30	88.6
13	7.8×10^9	4.4×10^8	210	40	113.7
14	5.2×10^9	4.4×10^8	210	40	105.9
15	7.8×10^9	4.4×10^8	210	20	119.2
16	6.5×10^9	5.9×10^8	320	50	130.6
17	7.8×10^9	4.4×10^8	430	20	129
18	5.2×10^9	4.4×10^8	430	20	88.7
19	6.5×10^9	8.9×10^8	320	30	169.5
20	6.5×10^9	5.9×10^8	320	30	137.8
21	6.5×10^9	5.9×10^8	320	30	135.6
22	5.2×10^9	7.4×10^8	430	40	78.2
23	6.5×10^9	5.9×10^8	320	30	136.3
24	5.2×10^9	7.4×10^8	210	20	90.8
25	6.5×10^9	5.9×10^8	320	10	90.3
26	5.2×10^9	4.4×10^8	210	20	91.5
27	7.8×10^9	7.4×10^8	210	40	141.7
28	3.9×10^9	5.9×10^8	320	30	80.1
29	7.8×10^9	7.4×10^8	430	40	133.6
30	7.8×10^9	7.4×10^8	430	20	148.2

Design−Expert software is applied to the bending damage force test results for quadratic regression fitting analysis. As shown in Table 5, the regression model $p = 0.0017 < 0.01$, which confirmed that the model was significant within the 95% confidence interval. Moreover, the coefficient of determination (R^2) and the adjusted coefficient of determination (R^2_{adj}) are 0.9453 and 0.9163 close to 1, respectively, indicating that the calculated model is in good agreement with the experimental data. The squared terms of normal stiffness X_1, shear stiffness X_2, and shear stiffness X_2 have a highly significant effect on the bending damage force, and the squared terms of normal contact stiffness X_1 and shear critical force X_3 have a significant effect on the bending damage force.

Table 5. Bending damage force response surface quadratic regression model analysis of variance.

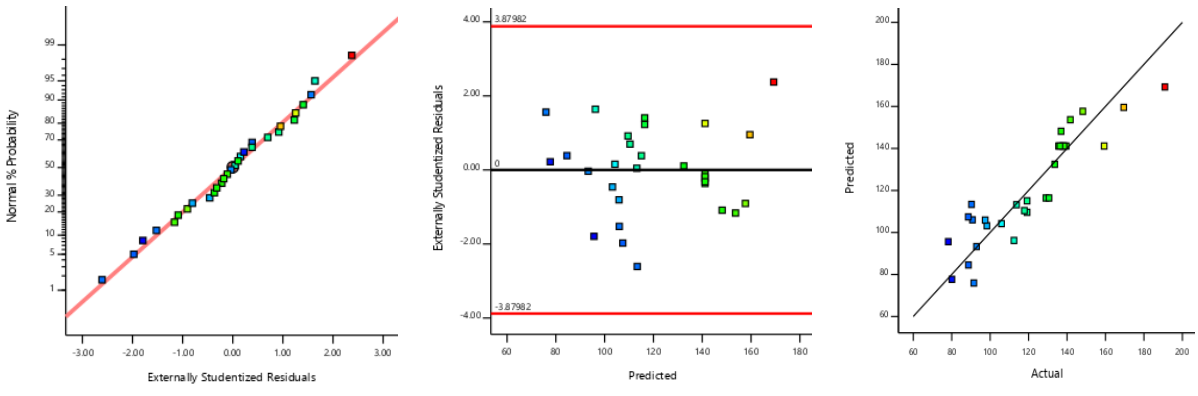
Source	Degree of Freedom	Mean Square	*F*	*p*
Model	14	1318.29	5.06	0.0017
X_1	1	7444.80	28.59	<0.0001 **
X_2	1	4074.22	15.65	0.0013 **
X_3	1	238.77	0.9170	0.3534
X_4	1	13.95	0.0536	0.8201
X_1X_2	1	877.64	3.37	0.0863
X_1X_3	1	3.15	0.0121	0.9139
X_1X_4	1	608.86	2.34	0.1470
X_2X_3	1	339.48	1.30	0.2714
X_2X_4	1	369.60	1.42	0.2520
X_3X_4	1	92.64	0.3558	0.5597
X_1^2	1	1364.48	5.24	0.0370 *
X_2^2	1	100.65	0.3866	0.5434
X_3^2	1	2961.33	11.37	0.0442 *
X_4^2	1	1182.38	4.54	0.0500
Intercept	15	260.37		
Residual				
Lack of fit	10	350.03	4.32	0.0600
Pure error	5	81.05		
Cor total	29			

Note: ** means highly significant ($p < 0.01$), * means significant ($0.01 \leq p < 0.05$).

Under the condition that the model is guaranteed to be significant and the misfit term is not significant, the quadratic regression model is optimized and adjusted to eliminate the insignificant terms normal critical force X_3 and shear critical force X_4 to establish the regression equation of straw skin parameters and bending damage force as follows:

$$F_1 = -428.01 + 6.06 \times 10^{-8} X_1 + 1.26 \times 10^{-7} X_2 - 4.17 \times 10^{-18} X_1^2 - 8.59 \times 10^{-16} X_3^2 \quad (2)$$

Figure 10 shows the residual diagnostic plot of the quadratic model, and Figure 10a demonstrates that the dispersion points are close to a straight line, indicating that the model is sufficient to describe the relationship between the independent variables and the straw bark damage force. Figure 10b shows the corresponding relationship between the residual error and the equation. The more scattered the discrete points, the more irregular they are, indicating that the prediction effect of this equation is better. Figure 10c shows the comparison between the predicted and experimental values of straw epidermal damage force. The linear distribution indicates that the model fits well and the model can analyze and predict the straw epidermal damage force.



(**a**) (**b**) (**c**)

Figure 10. Residual diagnostic map of the secondary model of straw outer bark. (**a**) Normal plot of residuals; (**b**) residuals vs. predicted; and (**c**) predicted vs. actual.

The calculation by the constraint solver tool of Design−Expert shows that when $X_1 = 6.8571 \times 10^9$ N/m and $X_2 = 5.2297 \times 10^8$ N/m, the simulated test damage force is 124.69 N, which is a 2.4% error from the average bending damage force of 127.8 N of the actual test. The bending damage curve of the epidermis is shown in Figure 11, which shows that the bending damage process of the epidermis is divided into three stages, including extrusion deformation, bending damage, and fracture stage. The epidermis in the actual test is tested by removing the inner flesh of the corn straw, retaining the outer bark of the straw can better ensure the mechanical properties of the epidermis itself cylindrical structure, and cutting the cylindrical structure of the destructive force at a greater force than the destructive force required for the lamellar structure. At the beginning of the test, the soft tissue of the epidermis is deformed, and the change in the damage force value is not obvious; with the increase in displacement, the epidermis is bent and damaged, and the damage force is linearly increased, and then the damage force increases slowly until it reaches the maximum value. At this stage, the internal tissues of the epidermis fractures successively until the bending damage force exceeds the binding strength of the vascular bundles of all epidermal tissues, causing the epidermis to fracture. The epidermal specimens used in this test are irregular hollow cylinders, and there are differences in the bending process in terms of the damage force applied to different parts, which may lead to fluctuations in the bending damage force and poor smoothness of the curve in the actual test.

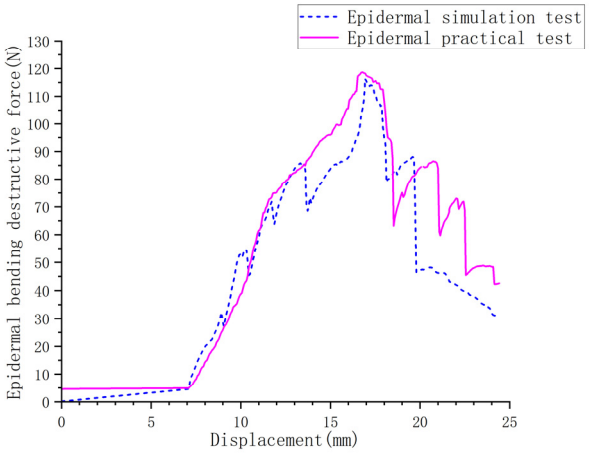
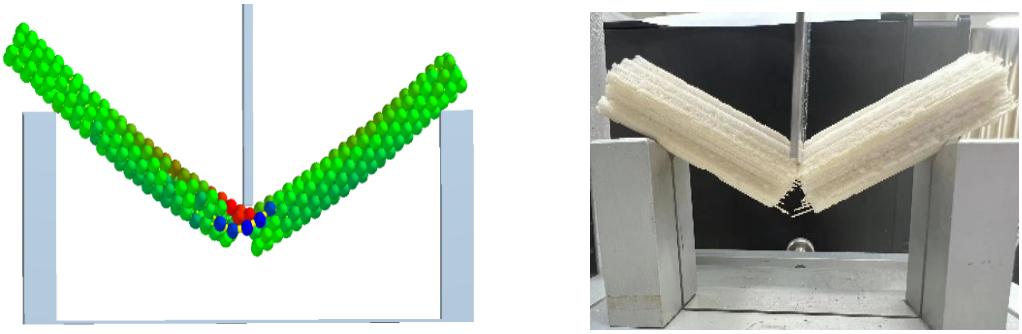


Figure 11. Comparison of bending damage force results of straw epidermis.

3.2. Optimization of Internal Binding Parameters of Corn Straw

The inner flesh of the corn straw is less hard compared to the epidermis, and the difference in cutting force between the dynamic and fixed knives cutting the epidermis and the inner flesh of the corn straw during the chopping process is large. Therefore, the bonding parameters of the inner flesh of the straw are calibrated. The shape of the inner flesh and the epidermis of the corn straw are close to circular in the cross−section, the sample shape of the epidermis bonding parameter calibration process is a hollow cylinder, the sample of the inner flesh bonding parameter calibration is a cylinder, and a simulated bending damage test is conducted, as shown in Figure 12.

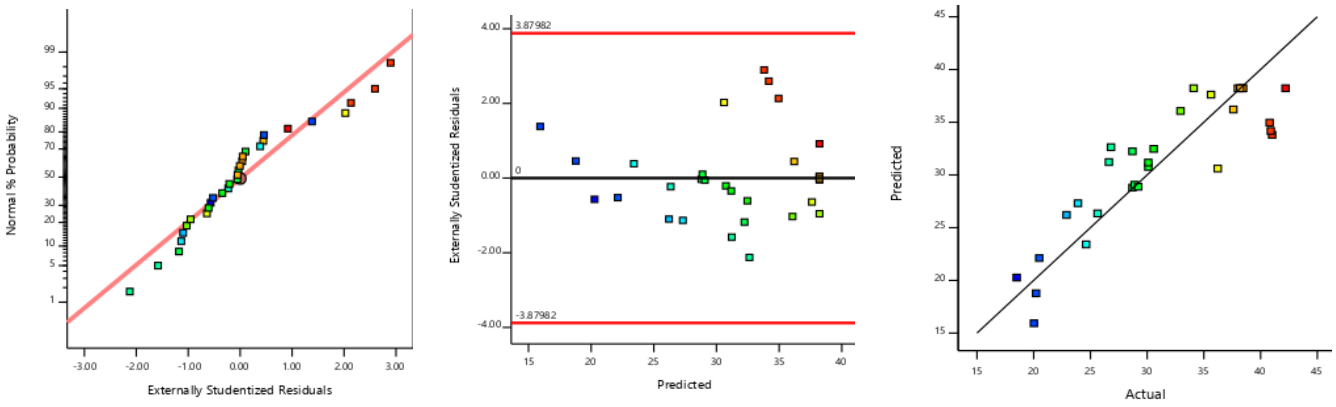


(**a**) (**b**)

Figure 12. Comparison of straw inner flesh bending test. (**a**) Discrete element bending test of straw inner flesh; (**b**) physical bending test of straw inner flesh.

With F_2 as the response value and X_5 (normal contact stiffness), X_6 (shear stiffness), X_7 (normal critical force), and X_8 (shear critical force) as the independent variables, the test codes for the independent variables of the inner flesh bonding parameters are shown in Table 6. The test protocols and results of the inner flesh bonding parameters are shown in Table 7.

According to the analysis of the inner flesh bending damage force response surface multivariate regression model variance results to obtain the factors affecting the inner flesh bending damage force, accuracy of the polynomial regression model on the premise of optimization adjustment to eliminate insignificant terms is ensured, as shown in Table 8. Among them, X_5 (normal contact stiffness) and X_6 (shear stiffness) have a very significant influence on bending destructive power. X_6^2 has a very significant influence on bending destructive power, and X_5^2 has a significant influence on bending destructive power. Furthermore, the coefficient of determination (R^2) and the adjusted coefficient of determination (R_{adj}^2) are 0.9380 and 0.9174 close to 1, respectively, indicating that the computational model agrees well with the experimental data. The model can be analyzed and predicted for the straw inner flesh damage force based on the residual diagnostic plot of the quadratic model of straw inner flesh, as shown in Figure 13.



(**a**) (**b**) (**c**)

Figure 13. Residual diagnostic plots of the quadratic model of the inner flesh of straw. (**a**) Normal plot of residuals; (**b**) residuals vs. predicted; (**c**) predicted vs. actual.

Table 6. Internal flesh bonding model parameter codes.

Code Value	Internal Flesh Bonding Model Parameters			
	X_5/(N·m^{-1})	X_6/(N·m^{-1})	X_7/MPa	X_8/MPa
−2	2×10^8	2.0×10^8	15	0.25
−1	3.8×10^8	3.0×10^8	25	0.35
0	5.6×10^8	4.0×10^8	35	0.45
1	7.4×10^8	5.0×10^8	45	0.55
2	9.2×10^8	6.0×10^8	55	0.65

Table 7. Experimental design and results of internal flesh bonding parameters.

Serial Number	X_5/(N·m^{-1})	X_6/(N·m^{-1})	X_7/MPa	X_8/MPa	Destructive Power (F_2)/N
1	5.6×10^8	4.0×10^8	35	0.45	34.1
2	3.8×10^8	3.0×10^8	25	0.55	30.1
3	7.4×10^8	3.0×10^8	45	0.35	35.63
4	7.4×10^8	3.0×10^8	25	0.55	28.7
5	3.8×10^8	5.0×10^8	25	0.55	22.89
6	5.6×10^8	4.0×10^8	15	0.45	28.9
7	2×10^8	4.0×10^8	35	0.45	24.62
8	3.8×10^8	3.0×10^8	45	0.55	30.58
9	9.2×10^8	4.0×10^8	35	0.45	40.8
10	5.6×10^8	4.0×10^8	35	0.45	38.2
11	7.4×10^8	3.0×10^8	45	0.55	26.81
12	5.6×10^8	4.0×10^8	35	0.45	38
13	5.6×10^8	4.0×10^8	35	0.45	38.45
14	5.6×10^8	4.0×10^8	35	0.65	40.9
15	5.6×10^8	4.0×10^8	35	0.25	29.21
16	7.4×10^8	5.0×10^8	45	0.55	26.63
17	7.4×10^8	5.0×10^8	25	0.35	23.9
18	5.6×10^8	4.0×10^8	55	0.45	41.02
19	3.8×10^8	3.0×10^8	25	0.35	25.63
20	5.6×10^8	4.0×10^8	35	0.45	42.2
21	5.6×10^8	2.0×10^8	35	0.45	36.22
22	3.8×10^8	3.0×10^8	45	0.35	32.94
23	5.6×10^8	6.0×10^8	35	0.45	20.21
24	3.8×10^8	5.0×10^8	45	0.55	20.49
25	7.4×10^8	3.0×10^8	25	0.35	28.7
26	3.8×10^8	5.0×10^8	25	0.35	20.02
27	7.4×10^8	5.0×10^8	25	0.55	37.6
28	3.8×10^8	5.0×10^8	45	0.35	18.5
29	7.4×10^8	5.0×10^8	45	0.35	30.1
30	5.6×10^8	4.0×10^8	35	0.45	38.4

Table 8. Analysis of variance of quadratic regression model of internal flesh bending damage force response surface.

Source	Degree of Freedom	Mean Square	*F*	*p*
Model	14	82.08	3.69	0.0085
X_5	1	199.99	8.99	0.0090 **
X_6	1	209.92	9.44	0.0077 **
X_7	1	33.56	1.51	0.2382
X_8	1	42.03	1.89	0.1894
X_5X_6	1	79.83	3.59	0.0776
X_5X_7	1	0.8100	0.0364	0.8512
X_5X_8	1	1.93	0.0869	0.7722
X_6X_7	1	28.94	1.30	0.2718
X_6X_8	1	29.70	1.34	0.2659
X_7X_8	1	70.98	3.19	0.0942
X_5^2	1	140.02	6.30	0.0241 *
X_6^2	1	313.93	14.12	0.0019 **
X_7^2	1	78.98	3.55	0.0790
X_8^2	1	76.78	3.45	0.0829
Intercept Residual	15	22.24		
Lack of fit	10	30.06	4.56	0.0539
Pure error	5	6.59		
Cor total	29			

Note: ** means highly significant ($p < 0.01$), * means significant ($0.01 \leq p < 0.05$).

Since X_7 (normal critical force) and X_8 (shear critical force) are not significant terms, the central horizontal values are 35 MPa and 0.45 MPa, respectively. The quadratic regression equation between the bending destructive power of inner flesh and the significant factors is obtained after the non−significant terms are removed.

$$F_2 = -106.68 + 5.76 \times 10^8 X_5 + 1.57 \times 10^7 X_6 - 6.97 \times 10^{17} X_5^2 - 3.38 \times 10^{16} X_6^2 \quad (3)$$

The calculation by the constraint solver tool of Design−Expert shows that when $X_5 = 7.2 \times 10^8$ N/m and $X_6 = 3.48 \times 10^8$ N/m, the simulated test damage force is 32.57 N, which is 1.6% error from the actual test average bending damage force of 28.14 N. The bending damage curve of the inner flesh is shown in Figure 14, which shows that the bending damage process of the inner flesh is divided into three stages, including extrusion deformation, bending damage, and fracture stage, which is similar to the bending damage trend of the epidermis. In order to ensure the inner flesh structure and mechanical properties, the inner flesh is obtained by cutting the external epidermal tissue, and the hardness of the inner flesh is low compared with the hardness of the epidermis, and the inner flesh contact point is deformed elastically after applying force, and gradually the internal fibers break. The curve fluctuation in the actual test bending test is produced by the gradual fracture of the fiber, not the internal fiber fracture at the same time. At the beginning of the test, the change in the damage force is small, but the resulting displacement is large. It is possible that this part of the curve reflects not the mechanical properties of the inner flesh, but the instability caused by the placement of the inner flesh specimen. With the increase in displacement, the bending damage force in the actual test and simulation test appears to decrease, the reason may be that the damage occurs at the weak position of the material inside the specimen, the damage force decreases rapidly, and then the damage force is assumed by the surrounding material and the damage force rises, and this process keeps repeating; when the damage force continues to increase to the peak, the inner flesh fractures and the damage force starts to decrease. The inner flesh cells are loose and porous, elastic, and the epidermal fiber tissue strength difference is obvious, so the destructive force of the inner flesh will not produce a sudden fracture.

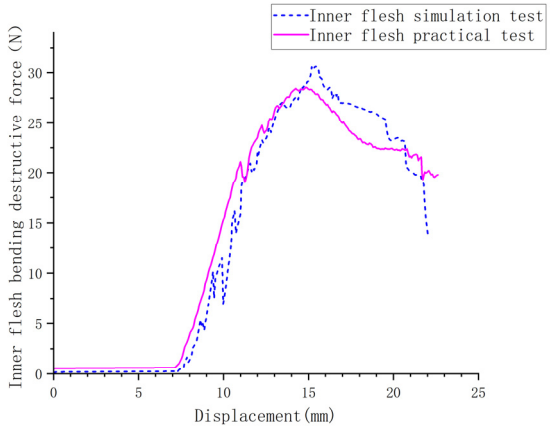
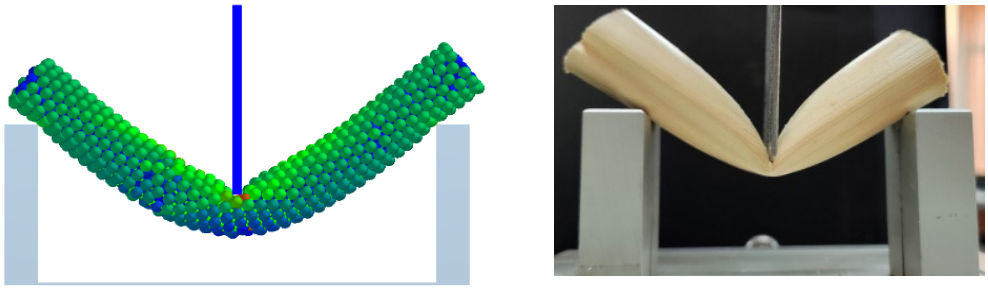


Figure 14. Comparison of the results of bending damage force in the inner flesh of straw.

3.3. Optimization of Bonding Parameters between Epidermis and Inner Flesh of Corn Straw

The epidermis and the inner flesh of the corn straw are not two independent individuals, but are connected to each other. The bond parameters of the epidermis and the inner flesh lacks in the present corn straw bond parameter calibration test. The bonding parameters between the epidermis and the inner flesh are calibrated by bending damage force tests on the whole corn straw, as shown in Figure 15.



(**a**) (**b**)

Figure 15. Whole straw bending test comparison. (**a**) Whole straw discrete element bending test; (**b**) whole straw physical bending test.

The calibration process of bonding parameters between epidermis and inner flesh is the same as the previous two calibration processes, with F_3 (bending damage force) as the response value, X_9 (normal contact stiffness), X_{10} (shear stiffness), X_{11} (normal critical force), and X_{12} (shear critical force) as the independent variables, coded according to the range of epidermal and inner flesh bonding parameters, as shown in Table 9, the number of repeat tests for the central group of epidermal and inner flesh bonding parameters test is six groups, the total number of tests is thirty groups, and the test protocol and results are shown in Table 10.

Table 9. Parameter codes of the epidermal and inner flesh bonding model.

Code Value	Bonding Parameters			
	X_9/(N·m^{-1})	X_{10}/(N·m^{-1})	X_{11}/MPa	X_{12}/MPa
−2	2×10^7	6×10^6	0.45	0.25
−1	3.5×10^8	1.95×10^7	0.50	0.30
0	5×10^8	3.3×10^7	0.55	0.35
1	6.5×10^8	4.65×10^7	0.60	0.40
2	6.5×10^8	6×10^7	0.65	0.45

Table 10. Experimental design and results of bonding parameters between epidermis and inner flesh.

Serial Number	X_9/(N·m^{-1})	X_{10}/(N·m^{-1})	X_{11}/MPa	X_{12}/MPa	Destructive Force (F_3)/N
1	5×10^8	4.65×10^7	0.5	0.3	280.4
2	2×10^8	4.65×10^7	0.6	0.3	302.4
3	2×10^8	4.65×10^7	0.5	0.3	302.2
4	3.5×10^8	3.3×10^7	0.55	0.35	298.2
5	3.5×10^8	3.3×10^7	0.45	0.35	296
6	5×10^8	4.65×10^7	0.6	0.3	269.3
7	5×10^8	4.65×10^7	0.5	0.4	310.9
8	3.5×10^8	3.3×10^7	0.55	0.25	285.4
9	3.5×10^8	3.3×10^7	0.55	0.45	329.2
10	3.5×10^8	3.3×10^7	0.65	0.35	250.9
11	5×10^8	4.65×10^7	0.6	0.4	308.9
12	3.5×10^8	3.3×10^7	0.55	0.35	293
13	2×10^8	4.65×10^7	0.5	0.4	280.2
14	5×10^8	1.95×10^7	0.5	0.4	329.8
15	2×10^8	1.95×10^7	0.6	0.3	257.5
16	5×10^8	1.95×10^7	0.6	0.3	246.5
17	2×10^8	1.95×10^7	0.5	0.4	313.8
18	3.5×10^8	6×10^7	0.55	0.35	278.2
19	5×10^7	3.3×10^7	0.55	0.35	287.7
20	3.5×10^8	6×10^7	0.55	0.35	278.4
21	2×10^8	1.95×10^7	0.6	0.4	278.3
22	6.5×10^8	3.3×10^7	0.55	0.35	310.3
23	3.5×10^8	3.3×10^7	0.55	0.35	281.2
24	5×10^8	1.95×10^7	0.6	0.4	280.3
25	3.5×10^8	3.3×10^7	0.55	0.35	308.9
26	2×10^8	4.65×10^7	0.6	0.4	288
27	3.5×10^8	3.3×10^7	0.55	0.35	274.9
28	2×10^8	1.95×10^7	0.5	0.3	307.7
29	3.5×10^8	3.3×10^7	0.55	0.35	306.8
30	5×10^8	1.95×10^7	0.5	0.3	279.1

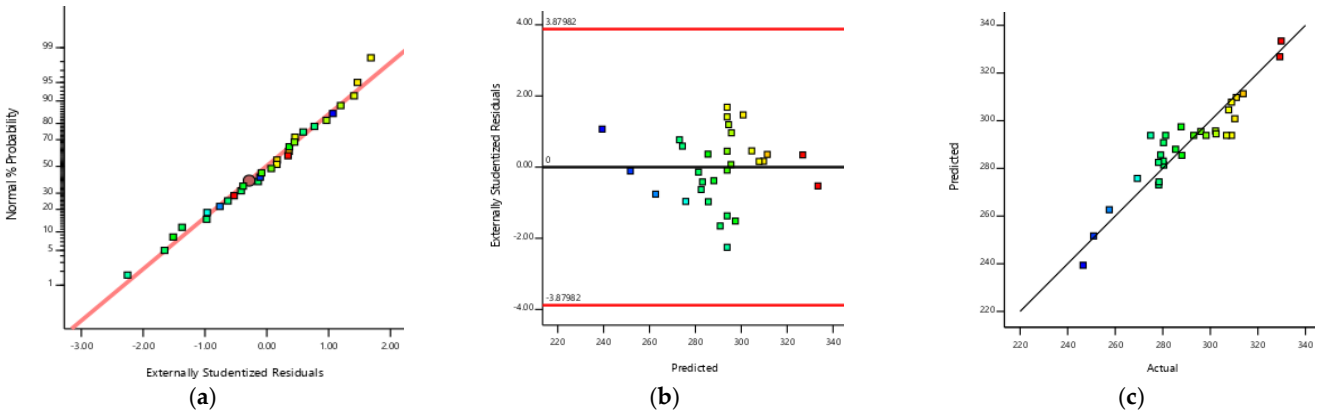
A quadratic regression fit analysis of the experimental design and results, as shown in Table 11, shows that X_{11} (normal critical force), X_{12} (shear critical force), a X_9X_{12}, $X_{10}X_{11}$ have a highly significant effect on the straw bending damage force, X_{11}^2 has a significant effect on the straw bending damage force, where X_9 (normal stiffness) and X_{10} (shear stiffness) and the squared terms of these two are insignificant, X_9X_{12} and $X_{10}X_{11}$ are significant, moreover, and the coefficient of determination (R^2) and the adjusted coefficient of determination (R_{adj}^2) are 0.9635 and 0.9364 close to 1, respectively, indicating that the calculated model agrees well with the experimental data. The model can be analyzed and predicted for the whole straw damage force based on the residual diagnostic plot analysis, as shown in Figure 16. The quadratic polynomial equation between each significant factor and the bending damage force F_3 after optimizing and adjusting the quadratic regression model with the guarantee of significant model and insignificant misfit term:

$$F_3 = 293.74 + 0.014X_{11} - 0.0012X_{12} + 1.37 \times 10^{12}X_9X_{12} + 1.51 \times 10^{11}X_{10}X_{11} - 2.03 \times 10^9X_{11}^2 \quad (4)$$

Table 11. Analysis of variance of the quadratic regression model for the response surface of the epidermis and flesh bending damage force.

Source	Degree of Freedom	Mean Square	*F*	*p*
Model	14	763.56	7.08	0.0003
X_9	1	17.17	0.1592	0.6955
X_{10}	1	99.63	0.9240	0.3517
X_{11}	1	2884.23	26.75	0.0001 **
X_{12}	1	2256.22	20.92	0.0004 **
X_9X_{10}	1	20.93	0.1941	0.6658
X_9X_{11}	1	19.14	0.1775	0.6795
X_9X_{12}	1	1683.05	15.61	0.0013 **
$X_{10}X_{11}$	1	1654.46	15.34	0.0014 **
$X_{10}X_{12}$	1	377.33	3.50	0.0810
$X_{11}X_{12}$	1	13.14	0.1219	0.7319
X_9^2	1	48.08	0.4459	0.5144
X_{10}^2	1	406.78	3.77	0.0711
X_{11}^2	1	703.25	6.52	0.0220 *
X_{12}^2	1	316.88	2.94	0.1071
Intercept Residual	15	107.83		
Lack of fit	10	68.45	0.3668	0.9168
Pure error	5	186.59		
Cor total	29			

Note: ** means highly significant ($p < 0.01$), * means significant ($0.01 \leq p < 0.05$).



(**a**) (**b**) (**c**)

Figure 16. Residual diagnostic plot of the whole straw quadratic model. (**a**) Normal plot of residuals; (**b**) residuals vs. predicted; and (**c**) predicted vs. actual.

The calculation by the constraint solver tool of Design−Expert shows that when $X_9 = 2.57 \times 10^8$ N/m, $X_{10} = 3.77 \times 10^7$ N/m, $X_{11} = 0.573$ MPa, and $X_{12} = 0.330$ MPa, the simulated test damage force is 288 N, and the error is 1.36%, with the actual test average bending damage force of 292 N.

The values of the bonding parameters are set in the Hertz-Mindlin with bonding module of the EDEM software according to the better parameter values obtained from the above simulation tests, as shown in Table 12.

Table 12. Whole straw bonding parameters.

Bonding Parameters	Epidermal Granules−Epidermal Granules	Core Granules−Core Granules	Core Granules−Epidermal Granules
Normal stiffness/(N·m^{-1})	6.88×10^9 N/m	7.2×10^8 N/m	2.57×10^8 N/m
Shear stiffness /(N·m^{-1})	4.74×10^8 N/m	3.48×10^8 N/m	3.77×10^7 N/m
Normal critical stress/Pa	3.79×10^8 Pa	3.5×10^7 Pa	5.73×10^5 Pa
Shear critical stress/Pa	3×10^7 Pa	4.5×10^5 Pa	3.3×10^5 Pa

The average value of bending damage force of corn straw is 288 N obtained from five repeated simulation tests under this combination of optimized parameter values, with a relative error of 1.36% from the bending damage force value of 292 N measured by actual physical tests. The bending damage curve of the whole corn straw is shown in Figure 17. The bending damage process of corn straw is divided into three stages, including extrusion deformation, bending damage, and fracture stage, which is similar to the bending damage trend of epidermis and inner flesh. Corn stalks in the actual bending breaking force test the epidermis by the inner flesh support role with the epidermis bending test different will not produce significant cracking, and the whole straw force curve increase rate is greater than the force curves of the skin and inner flesh increased at a rate greater than that of the skin and inner flesh. From the values of the bending damage force of corn straw, the maximum damage force of the whole corn straw is not simply the sum of the maximum damage force of the outer skin and the inner flesh, but is significantly greater than the sum of both. The reason may be that the applied bending force is also transferred between the different structures, and the bonded structure of the outer skin and inner flesh increases the strength of the corn straw when subjected to the breaking force, while acting as a buffer to avoid the phenomenon of collapse of the straw skin and sudden drop of the breaking force. Therefore, the epidermal and inner flesh bonding structures have a significant effect on the bending breaking force of the corn straw and should not be ignored.

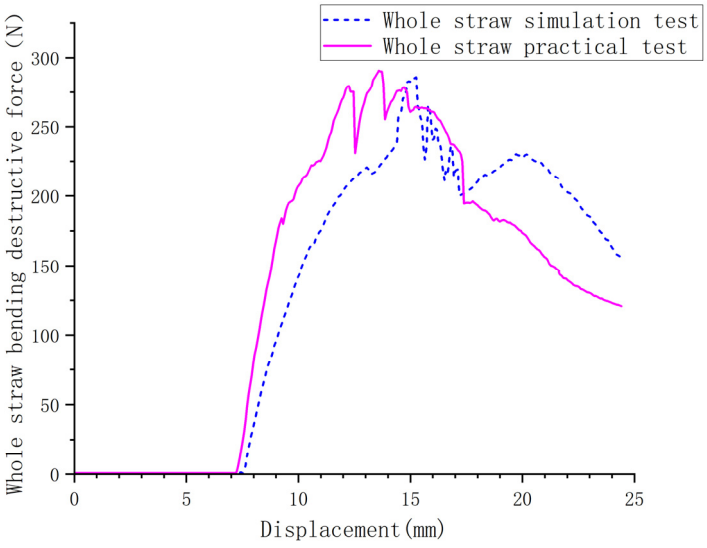


Figure 17. Comparison of bending damage force results for whole straws.

3.4. Control Test Analysis

The material throwing distances of the cutting and throwing device at different spindle speeds were obtained by fitting the material throwing trajectory coordinates using Origin 2019, as shown in Figure 18. The measured and simulated values of the corn straw throwing distances at four speeds of 600, 625, 650, 675, and 700 r/min are shown in Table 13, and the relative errors of the throwing distances are 6.1%, 5.5%, 6.4%, 6.3%, 5.8%, 6.3%, and 5.8%. The results show that the relative errors are within 7%. In the actual test, the air source

is wide and the airflow is complex, while in the discrete element simulation, the airflow in the external area of the machine is more stable than in the actual test. Therefore, the throwing distance of the actual test is larger than that of the simulation. Figure 18 compares the actual and simulated shredded sections of corn straw being cut and thrown outside the machine, and they are generally consistent.



(**a**) (**b**)

Figure 18. Comparison of shredded sections of corn straw. (**a**) Actual shredded section of corn straw; (**b**) simulated shredded section of corn straw.

Table 13. Test comparison and results.

Test Parameters		Shredder Speed r/min				
		600	**625**	**650**	**675**	**700**
Throwing distance *l*/(mm)	Simulation test	5410	5990	6280	6950	7510
	Bench test	5760	6340	6710	7420	7970
Relative error/%		6.1	5.5	6.4	6.3	5.8

4. Conclusions

- According to the structural mechanical characteristics of the corn straw, the crushing models of the whole corn straw, the skin of the straw, and the inside of the straw are established, and the grain bonding parameters are checked by combining with the bending destructive test, and the straw bonding parameters are obtained when the water content is 53~65%. The normal contact stiffness of the epidermis is 6.88×10^9 N/m, the shear stiffness of the epidermis is 4.74×10^8 N/m, the normal critical force of the epidermis is 379/MPa, the normal critical stress of the epidermis is 320 MPa, the shear critical stress of the epidermis is 30MPa, the normal stiffness of the inner flesh is 7.2×10^8 N/m, the shear stiffness of the inner flesh is 3.48×10^8 N/m, the normal critical stress of the inner flesh is 35 MPa, the shear critical stress of the inner flesh is 0.45 MPa, the normal stiffness of the epidermis-inner flesh is 2.57×10^8 N/m, the shear stiffness of the epidermal-inner flesh is 3.77×10^7 N/m, the normal critical stress of the epidermal-inner flesh is 0.573 MPa, and the shear critical stress of the epidermal-inner flesh is 0.33 MPa.
- The Hertz-Mindlin with bonding parameters obtained by parameter checking are used to carry out the simulation test of cutting and throwing, and the distance after cutting and throwing of corn straw is measured. Five kinds of throwing distances are obtained at the spindle speed of 600, 625, 650, 675, and 700 r/min. The corresponding throwing distance of each kind of speed is 5410, 5990, 6280, 6950, and 7510 mm, respectively.

- Experimental validation is performed for the simulation results. When the spindle speed is 600, 625, 650, 675, and 700 r/min, the corresponding throwing distances are 5760, 6340, 6710, 7420, and 7970 mm, respectively. The throwing distance of straw fragments increases with the increase in rotating speed, and the influence law is consistent with the actual test. The relative error between the simulation results and the actual test is less than 7%. Thus, it can be shown that the simulation model, as well as the parameters of corn straw, can be used for discrete element simulation experiments of cutting and throwing of corn straw.

This paper is limited by the simulation tools in the course of the study, the complex actual operation process is simplified, simulation and experimental studies are carried out on the straw breaking and cutting and throwing process for only five speeds, and there are some differences than the actual operation process. The Hertz-Mindlin with bonding model used in the study is applicable to the simulation of cutting and throwing of corn straw with different tissues and without knots, and further exploration and validation is needed when people use corn straw studies for other characteristics. The effect of nodal straw and blades on the throwing distance is ignored in the validation process. From the conclusion of the study, it can be seen that the study method in this paper is applicable to the simplified cutting and throwing process of corn straw, which can further enrich the means of structural optimization of the cutting and throwing straw processing machine and improve the efficiency of the processing machine and the quality of the straw shredding section with reference significance.

Author Contributions: Conceptualization, W.L. and W.Z.; methodology, W.L.; software, W.L.; validation, W.L., Q.S. and M.F.; formal analysis, W.Z.; investigation, Z.Y. and J.Z.; resources, Z.Y.; data curation, L.W., M.F. and Q.S.; writing—original draft preparation, W.L. and W.Z.; writing—review and editing, W.L. and Q.S.; visualization, W.L.; supervision, Z.Y.; project administration, J.Z. and W.Z.; funding, W.Z. All authors have read and agreed to the published version of the manuscript.

Funding: This research was supported by the National Natural Science Foundation of China (No. 51865047); Natural Science Foundation of Inner Mongolia Autonomous Region, No.2018MS05002; Inner Mongolia Agricultural University, No. NDYB2018−37; Natural Science Foundation of Inner Mongolia, No.2020BS05023.

Institutional Review Board Statement: Not applicable.

Informed Consent Statement: Not applicable.

Data Availability Statement: Not applicable.

Conflicts of Interest: The authors declare no conflict of interest.

References

1. Li, X.; Wang, Y.; Sun, Y.; Sun, C. Present situation of corn straw resources in China and research progress in feed conversion. *Feed. Res.* **2022**, *18*, 129–132.
2. Li, X.; Lu, Z.; Pu, Y.; Li, R.; Jia, Y.; Amirsalar, K.; Sui, W. Physicochemical properties and enzymatic digestibility of steam−exploded maize stalk under temperature−pressure decoupling. *Trans. CSAE* **2022**, *38*, 239–246.
3. Che, Y.; Xia, X.; He, B.; Gao, Y.; Ren, W.; Liu, H.; Liu, J.; Huang, T.; Han, W.; Lei, L. A corn straw−based diet increases release of inflammatory cytokines in peripheral blood mononuclear cells of dairy cows. *J. Zhejiang Univ. Sci. B* **2018**, *19*, 796–806. [CrossRef] [PubMed]
4. Li, X.; Du, Y.; Liu, L.; Zhang, Y.; Guo, D. Parameter calibration of corncob based on DEM. *Adv. Powder Technol.* **2022**, *33*, 103699. [CrossRef]
5. Ghodki, B.; Patel, M.; Namdeo, R.; Carpenter, G. Calibration of discrete element model parameters: Soybeans. *Comput. Part. Mech.* **2019**, *6*, 3–10. [CrossRef]
6. Chai, R.; Cheng, Q.; Chen, X.; Luo, L.; Ma, C.; Zhang, L.; Zhang, L.; Li, J.; Gao, H. Spatio−temporal variations of wheat, rice and maize straw in major grain−producing counties of Anhui Province and utilization potential of straw nutrient returning to field. *Trans. CSAE* **2021**, *37*, 234–247.
7. Guan, Z.; Mu, S.; Li, H.; Jiang, T.; Zhang, M.; Wu, C. Flexible DEM model development and parameter calibration for rape stem. *Appl. Sci.* **2022**, *12*, 8394. [CrossRef]

8. Hoseinian, S.; Hemmat, A.; Esehaghbeygi, A.; Shahgoli, G.; Baghbanan, A. Development of a dual sideway−share subsurface tillage implement: Part 1. Modeling tool interaction with soil using DEM. *Soil Tillage Res.* **2022**, *215*, 105201. [CrossRef]
9. Wang, L.; He, C. Water resistance and flexural properties of three nano−fillers reinforced corn straw polyvinyl chloride composites. *J. Adhes. Sci. Technol.* **2022**, *36*, 2199–2212. [CrossRef]
10. Yan, W.; Cui, W.; Qi, L. DEM study on the response of fresh concrete under vibration. *Granul. Matter* **2022**, *24*, 105–119. [CrossRef]
11. Benemerito, I.; Modenese, L.; Montefiori, E.; Mazzà, C.; Viceconti, M.; Lacroix, D.; Guo, L. An extended discrete element method for the estimation of contact pressure at the ankle joint during stance phase. *Proc. Inst. Mech. Eng. Part H: J. Eng. Med.* **2020**, *234*, 507–516. [CrossRef]
12. Kratky, L.; Jirout, T. Modelling of particle size characteristics and specific energy demand for mechanical size reduction of wheat straw by knife mill. *Biosyst. Eng.* **2020**, *197*, 32–44. [CrossRef]
13. Li, Y.; Li, B.; Jiang, Y.; Xu, C.; Zhou, B.; Niu, Q.; Li, C. Study on the dynamic cutting mechanism of green pepper (Zanthoxylum armatum) branches under optimal tool parameters. *Agriculture* **2022**, *12*, 1165. [CrossRef]
14. Ghodki, B.; Charith, K.; Goswami, T. Modeling breakage and motion of black pepper seeds in cryogenic mill. *Adv. Powder Technol.* **2018**, *29*, 1055–1071. [CrossRef]
15. Wu, K.; Song, Y. Research Progress Analysis of Crop Stalk Cutting Theory and Method. *Trans. Chin. Soc. Agric. Mach.* **2022**, *53*, 1–20.
16. Wang, W.; Zhu, C.; Chen, L.; Li, Z.; Huang, X.; Li, J. Design and experiment of active straw−removing anti−blocking device for maize no−tillage planter. *Trans. CSAE* **2017**, *33*, 10–17.
17. Zhao, S.; Gao, L.; Yuan, Y.; Hou, L.; Zhang, X.; Yang, Y. Maize straw motion law in subsoiling operation using discrete element method. *Trans. CSAE* **2021**, *37*, 53–62.
18. Wang, R.; Li, P.; Wang, T.; Wang, W.; Ren, T.; Li, L.; Li, S.; Sun, J. Discrete element parameter calibration for round bales of corn stalks. *J. Shenyang Agric. Univ.* **2022**, *53*, 319–326.
19. Fang, M.; Yu, Z.; Zhang, W.; Cao, J.; Liu, W. Friction coefficient calibration of corn stalk particle mixtures using Plackett−Burman design and response surface methodology. *Powder Technol.* **2022**, *396*, 731–742. [CrossRef]
20. Zhang, L.; Y, Z. Mechanical behavior of corn stalk pith: An experimental and modeling study. *INMATEH Agric. Eng.* **2017**, *51*, 39–48.
21. Wang, W.; Cai, D.; Xie, J.; Zhang, C.; Liu, L.; Chen, L. Parameters calibration of discrete element model for corn stalk powder compression simulation. *Trans. Chin. Soc. Agric. Mach.* **2021**, *52*, 127–134.
22. Hou, J.; Xie, F.; Wang, X.; Liu, D.; Chen, Z. Measurement of contact physical parameters of flexible rice straw and discrete element simulation calibration. *Acta Agric. Univ. Jiangxiensis* **2022**, *44*, 747–758.
23. Shi, R.; Dai, F.; Zhao, W.; Zhang, F.; Shi, L.; Guo, J. Establishment of discrete element flexible model and verification of contact parameters of flax stem. *Trans. CSAE* **2022**, *53*, 146–155.
24. Zhang, F.; Song, X.; Zhang, X.; Zhang, F.; Wei, W.; Dai, F. Simulation and experiment on mechanical characteristics of kneading and crushing process of corn straw. *Trans. Chin. Soc. Agric. Mach.* **2019**, *35*, 58–65.
25. Geng, D.; Mu, X.; Sun, Y.; Zhang, Y.; Li, H.; Jiang, H. Simulation and test of silage corn screw notched sawtooth type crushing roller. *Trans. CSAE* **2021**, *52*, 134–141.
26. Geng, D.; Sun, Y.; Mu, X.; Zhang, G.; Jiang, H.; Zhu, J. Simulation test and optimization of grain breakage of silage maize based on differential roller. *J. Jilin Univ.* **2022**, *52*, 693–702.
27. Weerasekara, N.S.; Powell, M.S.; Cleary, P.W.; Tavares, L.M.; Evertsson, M.; Morrison, R.D.; Quist, J.; Carvalho, R.M. The contribution of DEM to the science of comminution. *Powder Technol.* **2013**, *248*, 3–24. [CrossRef]
28. Li, J.; Liu, X.; Zou, L.; Yin, R.; Yang, K.; Yuan, J. Discrete element modeling method and experimental verification of spinach main−root. *Agric. Mech. Res.* **2021**, *43*, 181–185.
29. Cao, J. Mechanism and Energy Efficiency Characterization of High Efficiency Guillotine Chopper. Master's Thesis, Inner Mongolia Agricultural University, Hohhot, China, 6 July 2021.
30. Liu, W.; Yu, Z.; Cao, J.; Fang, M. Simulation analysis and experimental study on cutting performance of disc cutter chaff cutter. *Agric. Mech. Res.* **2023**, *45*, 150–155.
31. Tian, X.; Cong, X.; Qi, J.; Guo, H.; Li, M.; Fan, X. Parameter calibration of discrete element model for corn straw−soil mixture in black soil areas. *Trans. CSAE* **2021**, *52*, 100–108.
32. Gao, M.; Guo, K.; Yang, Z.; Li, X. Study on mechanical properties of corn stalk. *Trans. CSAE* **2003**, *34*, 47–49.

Disclaimer/Publisher's Note: The statements, opinions and data contained in all publications are solely those of the individual author(s) and contributor(s) and not of MDPI and/or the editor(s). MDPI and/or the editor(s) disclaim responsibility for any injury to people or property resulting from any ideas, methods, instructions or products referred to in the content.